

A Unified Framework for 10 TeV to EeV Diffuse Neutrino Sky and KM3-230213ASHIQI YU¹ AND B. THEODORE ZHANG^{2,3}¹*Department of Physics and Astronomy, University of Utah, Salt Lake City, Utah, USA*²*Key Laboratory of Particle Astrophysics and Experimental Physics Division and Computing Center, IHEP, CAS, China*³*TIANFU Cosmic Ray Research Center, Chengdu, Sichuan, China***ABSTRACT**

Establishing a unified origin that simultaneously accounts for the wide-band diffuse flux and recent ultra-high-energy (UHE) detections is a pressing challenge in multi-messenger astrophysics. Successive shock regimes in shock-breakout candidates, most notably low-luminosity gamma-ray bursts (LL GRBs), naturally introduce distinct physical environments producing a multi-component neutrino flux extending from 10 TeV to the UHE regime. Integrating prompt and afterglow phases within a unified dynamical framework yields a self-consistent explanation for this broadband emission. In this work, we discuss this framework, building on MWL observations. We show that the prompt emission from GRB 060218-like events accounts for $\gtrsim 10\%$ of the diffuse flux at 100 TeV, while GRB 100316D-like configurations predict a distinct flux peak near $10^{-9} \text{ GeV cm}^{-2} \text{ s}^{-1} \text{ sr}^{-1}$ at 100 PeV, providing a physical interpretation for the 220 PeV KM3-230213A event. This decoupling explains the lack of low-energy counterparts for individual UHE detections while maintaining consistency with the total diffuse neutrino flux. Ultimately, this framework identifies SBO-like LL GRBs as a unifying origin for these phenomena, providing a physical link across a wide band from 10 TeV to EeV energies testable by next-generation observatories, including GRAND, IceCube-Gen2, and RNO-G.

Keywords: Gamma-ray bursts (629) — Neutrino astronomy (1100) — Particle acceleration (1191) — Shocks (1451) — Transient sources (1851)

1. INTRODUCTION

Since the detection of high-energy astrophysical neutrinos began in 2013 (M. G. Aartsen et al. 2013), the physical mechanisms bridging the TeV and PeV regimes have challenged simple single-zone source models (N. Kurahashi et al. 2022). The observed diffuse neutrino flux (R. Abbasi et al. 2022a, 2025, 2021a; M. G. Aartsen et al. 2020, 2015; R. Naab et al. 2023) is well described by a broken power-law spectrum with mild structure at both low and high energies (R. Abbasi et al. 2025), likely arising from a combination of multiple astrophysical source populations and distinct emission phases within individual classes of transients.

Low-luminosity (LL) gamma-ray bursts (GRBs) constitute a distinct population within the GRB family and provide a compelling framework for neutrino production. Their high local event rate and mildly relativistic outflows, combined with the dense and compact environments of their progenitors, enable efficient cosmic-

ray acceleration and enhanced photohadronic interactions (e.g., S. Campana et al. 2006; A. M. Soderberg et al. 2006; Y.-Z. Fan et al. 2011). These properties distinguish them from high-luminosity (HL) GRBs, whose neutrino production efficiency is tightly constrained by stacking analyses, leaving their total contribution well below the observed IceCube diffuse flux (R. Abbasi et al. 2022b; K. Murase et al. 2022; S. Ai & H. Gao 2023; R.-Y. Liu et al. 2023). As a result, LL GRBs have long been considered promising contributors to the observed diffuse neutrino flux (e.g., K. Murase et al. 2006; N. Gupta & B. Zhang 2007; R.-Y. Liu et al. 2011; N. Senno et al. 2016; B. T. Zhang et al. 2018; D. Boncioli et al. 2019; S. Yoshida & K. Murase 2020, 2024).

A recent systematic study of neutrino emission from seven LL GRBs provided the first observational constraints on their physical parameters, including the cosmic-ray (CR) loading factor $\xi_{\text{cr}} \equiv L_{\text{cr}}/L_{\gamma, \text{iso}}$, the ratio between CR luminosity and isotropic-equivalent γ -ray luminosity. That analysis revealed an intrinsic diversity within the LL GRB population and highlighted the necessity of isolating physically distinct subclasses.

Among these, GRBs 060218 and 100316D are particularly representative. Both are associated with supernova and exhibit shock-breakout (SBO) signatures and similar energy partitioning among relativistic electrons, magnetic fields, and non-thermal protons (Paper I). This near-equipartition configuration naturally explains their prompt X-ray-dominated emission without invoking extreme microphysical parameters and suggests favorable conditions for efficient neutrino production.

In this work, we focus on these two SBO-associated LL GRBs. By fitting their prompt and afterglow multiwavelength spectra and light curves, we constrain the physical parameters governing particle acceleration and radiation in both phases and compute the resulting high-energy neutrino emission. We then evaluate the contribution of SBO-like LL GRBs to the diffuse neutrino flux. This framework provides population-level neutrino predictions grounded in multi-wavelength observation constrained models, enabling a quantitative assessment of the contribution of SBO-like LL GRBs to the diffuse neutrino flux with prompt and afterglow contributing to different energies self-consistently (Paper I). Remarkably, this unified approach also provides a physical basis for interpreting individual ultra-high-energy detections, such as the ~ 220 PeV neutrino recently reported by KM3NeT (O. Adriani et al. 2025a), which we discuss as a potential LL GRB afterglow event in Sec. 5.

2. MODELS AND METHODS

We model the multi-messenger emission from LL GRBs for both prompt and afterglow phases. Hadronic interactions and the resulting multiwavelength photon and neutrino spectra are simulated using the numerical code AMES (K. Murase et al. 2011; B. T. Zhang & K. Murase 2023; B. T. Zhang et al. 2025).

2.1. Models

For the prompt phase, we adopt the internal-shock framework from Paper I, assuming a single bulk-shock scenario consistent with SBO or mildly relativistic jet dissipation. The following discussion is focused on the afterglow modeling.

The expansion of the mildly relativistic ejecta into the circumburst medium (CBM) drives an external forward shock (FS) and reverse shock (RS). While the RS can contribute to early-time emission, it is typically sub-dominant in the multi-wavelength observations of the events considered here. Therefore, in this work, we focus on the FS as the primary site for the conversion of bulk kinetic energy into non-thermal particles (R. Sari & T. Piran 1995; P. Meszaros & M. J. Rees 1997; R. Sari et al. 1998). For GRB 060218 and

100316D, we adopt a wind-stratified CBM density profile ($n_{\text{CBM}} = 3 \times 10^{35} A_{\star} r^{-2}$) (R. B. Duran et al. 2015), where A_{\star} is the ratio of the mass-loss rate to the wind velocity, normalized to $10^{-5} M_{\odot} \text{ yr}^{-1} / 10^3 \text{ km s}^{-1}$. We treat the density normalization A_{\star} as a free parameter, adopting a prior range of [0.01, 5] consistent with Wolf-Rayet progenitors (R. A. Chevalier & Z.-Y. Li 2000).

For mildly-relativistic jets, the deceleration radius is $R_{\text{dec}} \simeq 2.7 \times 10^{15} \mathcal{E}_{k,51} \Gamma_{0,1}^{-2} A_{\star}^{-1} \text{ cm}$ and the ejecta spreading radius is $R_s \approx \Delta_0 \Gamma_0^2 \simeq 3 \times 10^{15} T_{\text{ej},3} \Gamma_{0,1}^2 \text{ cm}$ (B. Zhang 2018). The condition $R_s \gtrsim R_{\text{dec}}$ places these events in the thick-shell regime. We follow the standard evolution of the Lorentz factor and radius both during and after the shock crossing (P. Meszaros & M. J. Rees 1997; R. Sari et al. 1998; L. Nava et al. 2013). When the reverse shock finishes traversing the ejecta at the shock-crossing radius, $R_x \sim 1.6 \times 10^{15} \mathcal{E}_{k,51}^{1/2} T_{\text{ej},3}^{1/2} A_{\star}^{-1/2} \text{ cm}$, the Lorentz factor is $\Gamma_x \sim 6.1 \mathcal{E}_{k,51}^{1/4} T_{\text{ej},3}^{-1/4} A_{\star}^{-1/4}$, where the emission from the shock system reaches its peak.

The magnetic field strength within the shocked medium is estimated as $B_x \approx 7.9 \epsilon_{B,-4}^{1/2} \text{ G}$, assuming that a fraction ϵ_B of the post-shock internal energy density is partitioned into the magnetic field. We treat ϵ_B as a free parameter with a prior range of $[10^{-5}, 10^{-3}]$, a scale consistent with the values inferred from very-high-energy (VHE) observations of gamma-ray bursts (D. Miceli & L. Nava 2022). The maximum proton energy, limited by the dynamical timescale ($t_{\text{acc}} \approx t_{\text{dyn}}$) is $E_{p,\text{max}}^{\text{dyn}} \approx \eta^{-1} \Gamma_x Z e B_x (R_x / \Gamma_x) \sim 3.8 \times 10^{17} \epsilon_{B,-4}^{1/2} \eta_1^{-1} \text{ eV}$, where η is a numerical factor associated with the acceleration efficiency (L. Sironi et al. 2015).

In the afterglow phase, we assume that a fraction ϵ_e (ϵ_p) of the post-shock internal energy is carried by non-thermal electrons (protons) with a spectral index s_e (s_p). Given the lack of direct observational constraints on proton acceleration, we adopt typical values of $\epsilon_p = 0.1$ and $s_p = 2$. While the kinetic energy \mathcal{E}_k is estimated from the isotropic luminosity $10 \times L_{\gamma,\text{iso}} \times T_{90}$, we treat ϵ_e and s_e as free parameters. In this way, we break the inherent degeneracy between these variables, allowing the multiwavelength light curves (Fig. 1) to focus on constraining the shock environment and microphysics.

We then compute the high-energy neutrino production via photohadronic interactions between these protons and the synchrotron photon field. This framework ensures that the predicted neutrino flux is grounded in the observed shock evolution, which is constrained by the multi-wavelength data as discussed in the following subsection.

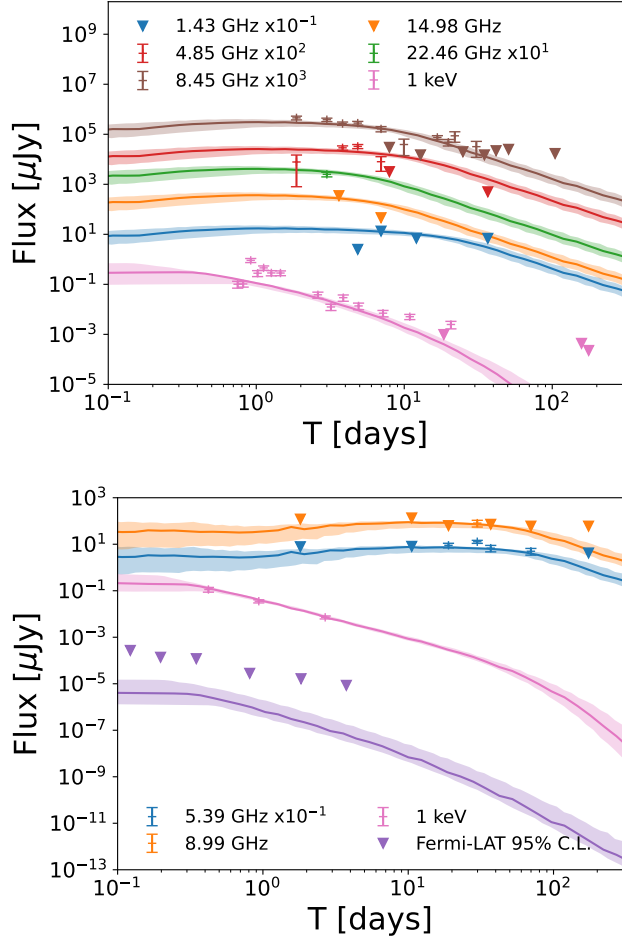


Figure 1. Multi-wavelength afterglow lightcurves for GRB 060218 (top) and GRB 100316D (bottom). Solid lines represent the posterior median of the FS model prediction, with 1σ uncertainties (shaded), compared against observations (crosses) with 1σ error bars or 95% C.L. upper limits (triangles). The *Fermi*-LAT upper limit is evaluated at 1 GeV.

2.2. Method

Given that GRB 060218 and GRB 100316D exhibit similar prompt phase properties as SBO candidates, we perform a joint spectral fit to constrain the shared model parameters. We employ a Markov Chain Monte Carlo (MCMC) approach to sample the posterior probability distributions, utilizing the multi-wavelength prompt observations (following the methods and observations detailed in Paper I). The resulting parameter constraints are summarized in Table 1, while the corresponding confidence contours illustrating parameter correlations are provided in Appendix B.

In contrast, the afterglow emission is governed by the interaction of the ejecta with the circumburst medium. Because this phase is sensitive to the unique external environment and initial ejecta properties of each burst,

we perform separate fits for the FS evolution of GRB 060218 and GRB 100316D. We apply our MCMC framework to their respective multi-wavelength light curves, incorporating radio, X-ray, and gamma-ray observations. The resulting parameter constraints are summarized in Table 4, and more details about the analysis can be found in Appendix A.

This framework ensures that the total neutrino output is consistently anchored to multi-wavelength observations. In the external FS region, the larger emission radius leads to lower magnetic field strengths and target photon densities compared to the prompt phase. This environment allows particles to reach the UHE regime more efficiently than in internal shock models (E. Waxman & J. Bahcall 1997). Consequently, the prompt and afterglow generated neutrino components naturally separate and populationally contribute to different regimes of the diffuse neutrino flux, as shown and discussed in the following sections.

Throughout this work, we adopt a flat Λ CDM cosmology with $H_0 = 67.3 \text{ km s}^{-1} \text{ Mpc}^{-1}$, $\Omega_M = 0.315$, and $\Omega_\Lambda = 0.685$ (S. Navas et al. 2024).

3. FIT RESULTS

Table 1. Inferred parameter values for the prompt phase model. Values represent posterior medians with 1D marginalized 1σ highest posterior density (HPD) uncertainty ranges and corresponding prior bounds.

Parameter	Median	1σ uncertainty	Prior range
$\log \xi_B$	2.0	[1.62, 3.00]	[-3.0, 3.0]
$\log \xi_e$	0.8	[0.51, 1.15]	[-0.5, 2.0]
$\log(R/\text{cm})$	13.0	[11.50, 13.84]	[11.5, 16]
Γ_0	7.9	[2.00, 11.14]	[2.0, 20.0]
s_e	2.4	[2.02, 2.59]	[2.0, 3.0]
ϵ_e	0.1	[0.01, 0.20]	[0.01, 0.3]
$\log \xi_p$	-0.4	[-2.00, 0.25]	[-2.0, 2.0]

Table 2. Afterglow model parameters for GRB 060218 and GRB 100316D. Values represent posterior medians with 1D marginalized 1σ HPD credible intervals, with prior ranges provided for reference.

Parameter	060218	100316D	Prior range
$\log(\epsilon_e)$	$-1.2^{+0.25}_{-0.33}$	$-0.7^{+0.37}_{-0.14}$	[-2.0, -0.3]
$\log(\xi_B)$	$-3.4^{+0.50}_{-0.45}$	$-3.5^{+0.31}_{-0.35}$	[-5.0, -0.3]
s_e	$2.1^{+0.01}_{-0.02}$	$2.3^{+0.06}_{-0.06}$	[2.05, 2.6]
Γ_0	$3.2^{+0.46}_{-0.70}$	$2.3^{+0.16}_{-0.24}$	[2.0, 5.0]
f_e	$-1.8^{+0.07}_{-0.18}$	$-1.7^{+0.18}_{-0.15}$	[-2, -0.3]
A_*	$0.5^{+0.33}_{-0.45}$	$4.3^{+0.67}_{-0.34}$	[0.01, 5]

For the prompt model, the joint fit reflects the shared physical properties of the SBO-like LL GRBs. The electron spectral index, $s_e \sim 2.4$, is consistent with the diffusive shock acceleration (DSA) scenario (L. Sironi et al. 2015), while the energy partition fractions for electrons and magnetic fields ($\log \xi_e \approx 0.8$, $\log \xi_B \approx 2.0$) suggest near-equipartition and efficient particle acceleration as discussed in detail in *Paper I*. The CR loading parameter, $\log \xi_p \approx -0.4$, is associated with the normalization of the neutrino production during the prompt emission phase.

The initial bulk Lorentz factor in our prompt model, Γ_0 , is weakly constrained with a median of 7.9 and a broad 1σ range of [2.00, 11.14]. This is expected under the bulk-shock scenario. Observed multi-wavelength light curves in the afterglow phase provide a better constraint to break the degeneracy between the emission radius and the expansion velocity (Table 2). We find Γ_0 values of $2.3^{+0.16}_{-0.24}$ for GRB 100316D and $3.2^{+0.46}_{-0.70}$ for GRB 060218, consistent with the mildly-relativistic expansion speeds expected for SBO driven LL GRBs. Additionally, our results yield energy partition fractions that are consistent across both bursts ($\log \epsilon_e \approx -1$, $\log \epsilon_B \approx -3.5$). These values align with standard FS models for LL GRBs (D. Miceli & L. Nava 2022). The spectral index of accelerated electrons agrees with the DSA scenario ($2.1^{+0.01}_{-0.02}$ for 060218 and $2.3^{+0.06}_{-0.06}$ for 100316D). The inferred circumburst densities suggest diverse wind-like environments, with $A_* \approx 0.5^{+0.33}_{-0.45}$ for GRB 060218 and $A_* \approx 4.3^{+0.67}_{-0.34}$ for GRB 100316D. These values are consistent with the ranges expected for the Wolf-Rayet star progenitors typically associated with LL GRBs (S. Campana et al. 2006; R. Margutti et al. 2013).

Our results show that while the prompt emission is determined by the internal conditions of the sources, the afterglow evolution reflects the diversity in circumburst densities and ejecta energetics. Anchored on multi-wavelength observations, our results establish a physical basis for the contribution of SBO-like LL GRBs to the high-energy neutrino sky, which is discussed next.

4. CONTRIBUTION TO DIFFUSE NEUTRINOS

The cumulative diffuse neutrino flux from the LL GRB population is calculated as:

$$E_\nu^2 \Phi_\nu = \frac{c}{4\pi H_0} \int_{z_{\min}}^{z_{\max}} dz \int_{L_{\min}}^{L_{\max}} dL_\gamma \frac{1}{(1+z)^2} \times \frac{d\rho_{\text{LL}}(z)/dL_\gamma}{\sqrt{\Omega_M(1+z)^3 + \Omega_\Lambda}} \left(E'_\nu^2 \frac{dN_\nu}{dE'_\nu} \right), \quad (1)$$

where dN_ν/dE'_ν represents the neutrino spectrum predicted by our models using the posterior medians of

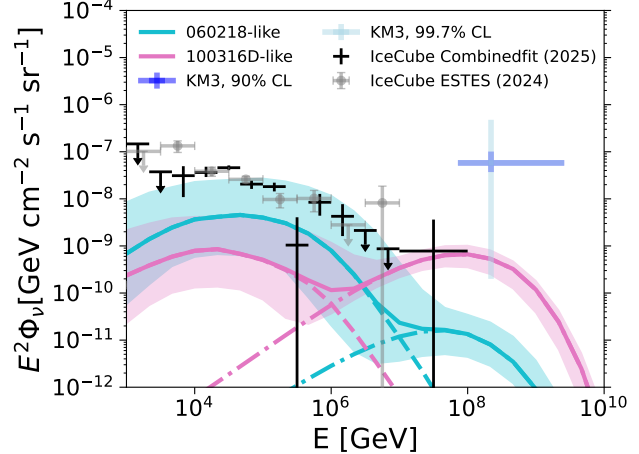


Figure 2. Predicted diffuse neutrino flux (solid lines) with 1σ uncertainties (shaded regions) from the SBO-like LL GRB population compared to observed astrophysical neutrino fluxes (crosses) (R. Abbasi et al. 2024, 2025; O. Adriani et al. 2025a). Scenarios assume a population composed of either GRB 060218-like (blue) or GRB 100316D-like (pink) sources. The prompt (dashed) and afterglow (dotted-dashed) sub-components are shown separately, highlighting the distinct contributions to the characteristic two-hump spectral distribution.

the parameters, and $E'_\nu = (1+z)E_\nu$. For the afterglow phase, the neutrino fluence is integrated from $T = 1000$ s to $T = 3 \times 10^7$ s to capture the full evolution of the FS. We adopt redshift limits of $z_{\min} = 0.001$ and $z_{\max} = 5$, with a luminosity range of $L_{\min} = 10^{46}$ to $L_{\max} = 10^{50}$ erg s $^{-1}$.

We adopt the luminosity function (LF) for SBO-like LL GRBs as a single power law with a spectral index of 0.84 and a local event rate of $\rho_0 \sim 164$ Gpc $^{-3}$ yr $^{-1}$ erg $^{-1}$ for luminosities above 5×10^{46} erg s $^{-1}$ (H. Sun et al. 2022). While alternative LFs (E. Liang et al. 2007; H. Sun et al. 2015) show a negligible impact on the diffuse flux, recent detections by the *Einstein Probe* (H. Hamidani et al. 2025) suggest a sample of SBO candidates that will further refine these population statistics and the resulting neutrino flux predictions.

The resulting diffuse neutrino flux spectrum (see Fig. 2) exhibits a characteristic two-hump structure, reflecting the distinct physical regimes of the prompt and afterglow phases. In an optimistic scenario, the prompt emission can explain more than $\sim 10\%$ of the diffuse flux at 100 TeV for a GRB 060218-like configuration. In comparison, the UHE component is highly sensitive to the circumburst environment. For instance, the dense stellar wind inferred for GRB 100316D enhances hadronic interaction efficiency, yielding a significantly higher afterglow-to-prompt flux ratio compared

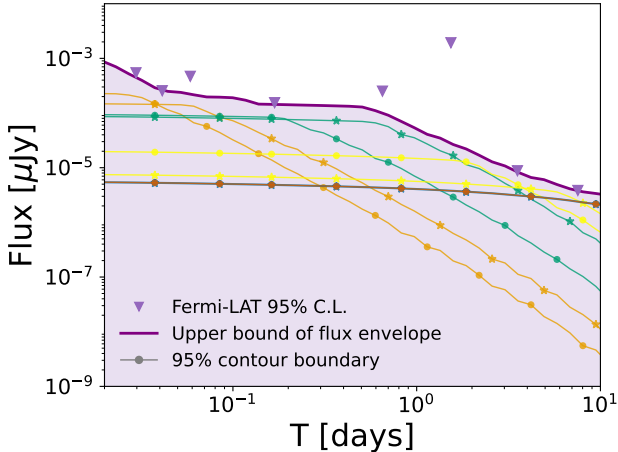


Figure 3. Predicted gamma ray flux representing the post-burn-in posterior parameter space for a hypothetical SBO-like LL GRB. The solid purple curve highlights the maximum predicted flux compared against the observed 95% confidence level upper limits from *Fermi*-LAT. The colored curves represent the parameter points along the 95% contour boundary, with colors and markers matching those in Fig. 4.

to the GRB 060218-like configuration. This secondary peak reaches the diffuse neutrino flux required to produce the highest energy neutrino detected to date, KM3-230213A.

5. UHE NEUTRINO DETECTION

The 220 PeV neutrino detected by KM3NeT (KM3-230213A) poses a challenge for standard astrophysical source models in explaining particle acceleration to such energies without violating existing observational constraints (S. Aiello et al. 2025). We propose that our SBO-like LL GRB framework naturally resolves this tension. Since the absence of multi-messenger signals suggests an intrinsically faint or cosmologically distant source, this event is likely a UHE neutrino produced in the afterglow phase while the prompt emission remains below detection thresholds.

To test this hypothesis, we adopt the posterior median parameters of GRB 100316D (from Table 2). Assuming a prompt duration of 1 ks and a jet onset at $T_0 - 3$ ks, we derive constraints on the distance and luminosity of the hypothetical LL GRB. We find that this SBO-like scenario is consistent with *Fermi*-LAT observations (see Fig. 3), with posterior medians of redshift $z \sim 0.18$ and isotropic luminosity $L_{\gamma, \text{iso}} \sim 10^{47.1} \text{ erg s}^{-1}$ (see Fig. 4 in Appendix B).

While the absence of photon signals and low-energy neutrinos is expected for such faint sources, the lack of signal compatible with a point-like source hypothesis (O. Adriani et al. 2025b) can be a consequence of the low

expected event rate from a potential SBO-like LL GRB. In our framework, the KM3-230213A event represents a rare, stochastic detection. Despite the larger effective area of IceCube, the low flux produced during the afterglow phase ensures that a single detection in KM3NeT remains statistically compatible with null results elsewhere.

6. SUMMARY AND DISCUSSIONS

In this work, we have established a multi-messenger framework to evaluate the contribution of SBO-like LL GRBs to the diffuse neutrino background. By anchoring our models to multi-wavelength observations of the SBO candidates GRB 060218 and GRB 100316D, we demonstrate that this single source class can naturally account for a multi-component neutrino spectrum spanning from 10 TeV to EeV. However, the two sources represent distinct regimes: the GRB 060218 configuration provides a significant flux of ~ 100 TeV neutrinos during the prompt phase but lacks a substantial UHE component. Conversely, the GRB 100316D configuration contributes effectively to the UHE neutrino sky but remains inefficient at energies below 1 PeV. To account for the entire observed energy range of diffuse neutrinos, the diversity in the inferred parameter space must be satisfied across this population, especially the properties of circumstellar material for the UHE regime.

A central conclusion of this work is that the distinct spectral regimes observed in the diffuse flux are intrinsic features of the same physical event. While the prompt and afterglow phases share a common central engine, their respective neutrino production efficiencies are governed by independent physical parameters. Consequently, individual events do not necessarily manifest as broadband power-law emitters. Instead, the non-power-law nature of the spectrum allows a source in a low-density environment to produce a detectable prompt signal without a corresponding UHE afterglow component. Conversely, this explains the occurrence of a UHE neutrino, such as the ~ 220 PeV KM3NeT event, where the afterglow flux is detectable even if the prompt-phase emission remains below sensitivity thresholds.

While our analysis focuses on SBO-like LL GRBs, these results establish a broader physical principle: any transient hosting successive shock regimes can naturally produce a multi-hump neutrino spectrum. Specifically, our framework demonstrates that the co-existence of internal and external shocks, or analogous distinct dissipation processes within a single engine, provides a universal mechanism for bridging the TeV to EeV regimes. This suggests that the observed diffuse flux may contain contributions from various transient populations,

such as stripped-envelope supernovae (R. Sawada & Y. Ashida 2025) or low-luminosity jets, provided they undergo similar dynamical evolution. While the potential contribution of these other classes remains to be quantified in future studies, the characteristic UHE-hump identified here serves as a concrete prediction for the SBO-like LL GRB population. Using the publicly available effective areas for GRAND (J. Álvarez-Muñiz et al. 2020), IceCube-Gen2 (R. Abbasi et al. 2021b; C. Glaser et al. 2020), and RNO-G J. A. Aguilar et al. (2021), we estimate the integrated detection rates of afterglow phase over a 10-year period (see Table 3).

Table 3. Projected number of events for future detectors: GRAND, IceCube-Gen2, and RNO-G over 10-year livetime for GRB 060218 and GRB 100316 configurations.

Event	Detector	Medium	Low	High
060218	GRAND	0.283	0.096	0.849
	IceCube-Gen2	0.093	0.030	0.342
	RNO-G	0.002	0.001	0.007
100316D	GRAND	19.467	8.674	29.711
	IceCube-Gen2	5.547	2.564	8.532
	RNO-G	0.105	0.049	0.162

We note that the peak neutrino fluence from a single external FS is approximately 10^{-6} GeV cm $^{-2}$, which is

roughly five orders of magnitude below the point-source sensitivity thresholds of upcoming radio-based UHE experiments (K. Kotera et al. 2025). Consequently, while individual event associations remain challenging, the next generation of large-scale neutrino telescopes will be uniquely positioned to test this model by searching for the predicted multi-component spectral signature in the UHE regime.

The future of this paradigm depends on expanding the sample of soft X-ray transients through facilities like the Einstein Probe (W. Yuan et al. 2025). Rapid multi-wavelength follow-up, particularly in the radio band, can be used to estimate the wind density of the circumstellar medium. Furthermore, future neutrino telescopes will reach the sensitivity required to reveal the secondary UHE peak, clarifying the role of LL GRBs as primary cosmic accelerators in the high-energy sky.

ACKNOWLEDGMENTS

B.T.Z. is supported in China by National Key R&D program of China under the grant 2024YFA1611402. We acknowledge the Center for High Performance Computing (CHPC) at the University of Utah for providing computational resources. Correspondence and requests for materials should be addressed to S.Y and B.T.Z.

APPENDIX

A. MULTI-WAVELENGTH OBSERVATIONS

Observations for the prompt phase are identical to those used in Paper I. For the afterglow phase, we use multi-wavelength data from radio, X-ray, and γ -ray observations, summarized in Table 4.

For GRB 060218, only the measured fluxes at 4.86, 8.46, and 22.5 GHz from VLA (A. M. Soderberg et al. 2006) are included in the fit, while all upper-limit points, including 1.43 GHz, are shown in the plots for comparison and completeness (see Fig. 1). For GRB 100316D, ATCA radio data at 5.4 and 9 GHz (R. Margutti et al. 2013) are used in the analysis. X-ray light curves are obtained from the *Swift*-XRT repository (P. A. Evans et al. 2009)⁴ when available.

For GRB 100316D and KM3-230213A, archival *Fermi*-LAT γ -ray data (1–300 GeV) are analyzed using the `fermipy` (v1.4.0) framework. We select `evtype==1` (FRONT) events within a 20° region of interest (ROI) centered on the target location. To ensure a robust background model, we first perform a broadband likelihood fit over a 20-day baseline following the trigger time. During this optimization, the normalizations of the Galactic (`gll_iem_v07`) and isotropic (`iso_P8R3_SOURCE_V3_v1`) diffuse components, as well as all point sources within 5° (including the target), are left free. Subsequently, the afterglow light curve is extracted with all background parameters fixed and the target photon index fixed at $\Gamma = 2$. For GRB 100316D, the analysis window spans $T_{90} + 3$ ks to 5 days post-trigger to exclude prompt emission. For KM3-230213A, the light curve analysis starts at $T_0 - 1$ ks to isolate the afterglow-dominated regime,

⁴ https://www.swift.ac.uk/xrt_spectra/

extending to $T_0 + 10$ days for broader temporal coverage, as the only observation dataset in the analysis. Given no significant signals are detected in any interval ($TS < 9$), we extract 95% confidence level upper limits for both events.

Table 4. Multi-wavelength observations used for afterglow fitting of GRBs 060218 and 100316D.

Band	GRB 060218	GRB 100316D	Telescope	Reference
Radio	1.43	—	VLA	A. M. Soderberg et al. (2006)
	4.86	—	VLA	
	8.46	—	VLA	
	22.5	—	VLA	
	—	5.4	ATCA	
X-ray	0.3–10 keV 00191157053	0.3–10 keV 00416135019	<i>Swift</i> -XRT Observation ID	R. Margutti et al. (2013)
γ-ray	—	1–300 GeV	<i>Fermi</i> -LAT	S. Abdollahi et al. (2022)

B. CONTOUR PLOTS

The confidence contours for the prompt phase joint fit of SBO-like GRBs 060218 and 100316D LL GRB are presented in Fig. 4 (left panel). Additionally, Fig. 5 shows the posterior contours for fitting the afterglow light curves of each event. In the right panel of Fig. 4, the constraints on $L_{\gamma, \text{iso}}$ and z derived from the *Fermi*-LAT upper limits present a median redshift of $z \gtrsim 0.18$, assuming the GRB 100316D configuration, as discussed in Sec. 5.

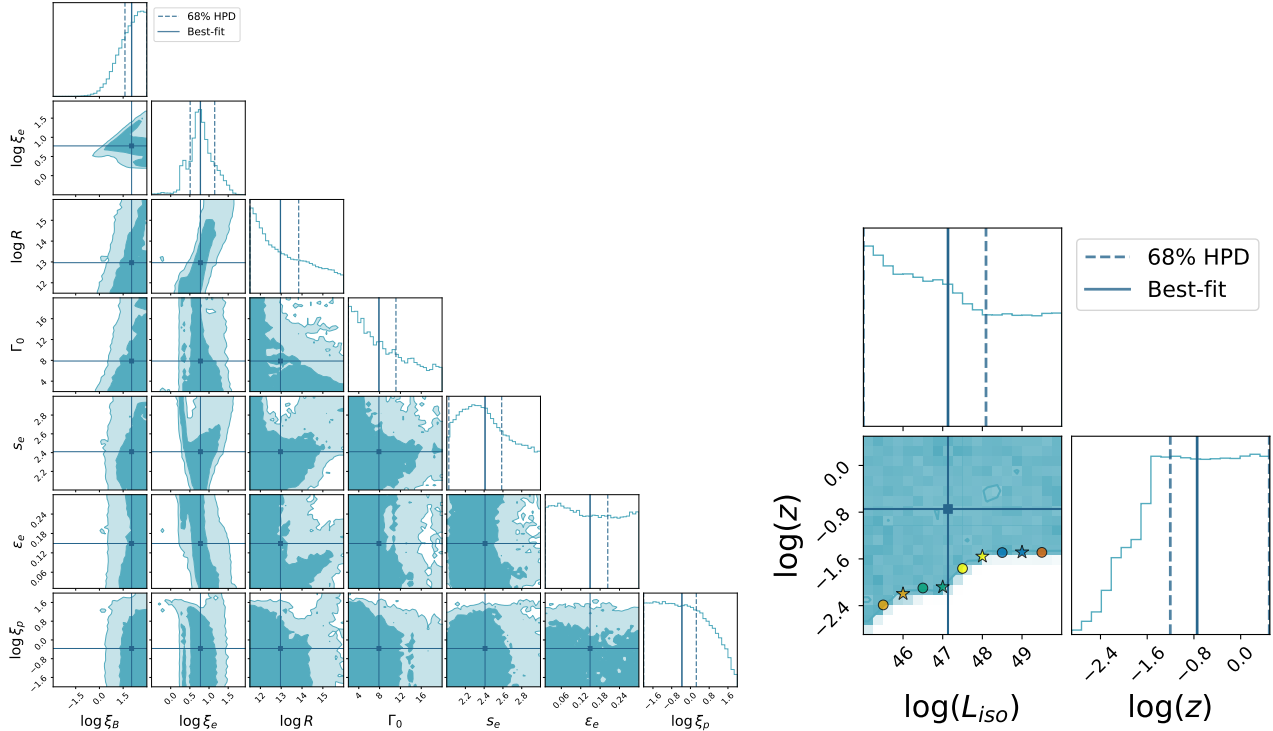


Figure 4. Left: Confidence contours of the joint spectral fitting parameters for the prompt phase. Crossing points indicate the medians of the post-burn-in MCMC samples, while dashed lines mark the 1σ HPD interval of the marginalized 1D posterior distribution. Best-fit values are provided in Table 1. Right: 95% posterior region in the isotropic gamma-ray luminosity ($L_{\gamma, \text{iso}}$) and redshift (z) parameter space for a hypothetical LL GRB with a GRB 100316D configuration. Stars represent parameter points at the boundary used to illustrate the predicted flux in Fig. 3. Solid lines indicate the posterior median, while the 68% HPD boundaries are shown as dashed lines.

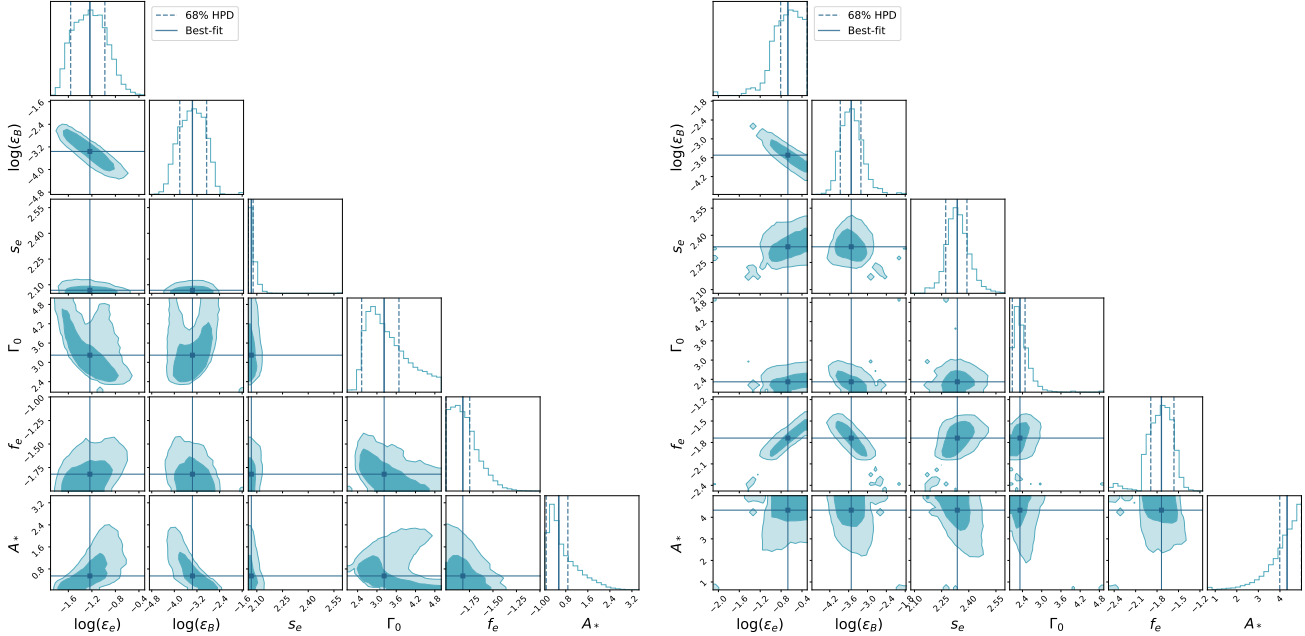


Figure 5. Confidence contours of the spectral fitting parameters for GRB 060218 (left) and GRB 100316D (right). Solid lines indicate the medians of the post-burn-in MCMC samples, while dashed lines mark the 1σ HPD interval of the marginalized 1D posterior distribution. Best fit values are provided in Table 2.

REFERENCES

Aartsen, M. G., et al. 2013, *Science*, 342, 1242856, doi: [10.1126/science.1242856](https://doi.org/10.1126/science.1242856)

Aartsen, M. G., Abraham, K., Ackermann, M., et al. 2015, *The Astrophysical Journal*, 809, 98, doi: [10.1088/0004-637X/809/1/98](https://doi.org/10.1088/0004-637X/809/1/98)

Aartsen, M. G., Ackermann, M., Adams, J., et al. 2020, *Phys. Rev. Lett.*, 125, 121104, doi: [10.1103/PhysRevLett.125.121104](https://doi.org/10.1103/PhysRevLett.125.121104)

Abbasi, R., Ackermann, M., Adams, J., et al. 2021a, *Phys. Rev. D*, 104, 022002, doi: [10.1103/PhysRevD.104.022002](https://doi.org/10.1103/PhysRevD.104.022002)

Abbasi, R., et al. 2021b, PoS, ICRC2021, 1183, doi: [10.22323/1.395.1183](https://doi.org/10.22323/1.395.1183)

Abbasi, R., Ackermann, M., Adams, J., et al. 2022a, *The Astrophysical Journal*, 928, 50, doi: [10.3847/1538-4357/ac4d29](https://doi.org/10.3847/1538-4357/ac4d29)

Abbasi, R., et al. 2022b, *Astrophys. J.*, 939, 116, doi: [10.3847/1538-4357/ac9785](https://doi.org/10.3847/1538-4357/ac9785)

Abbasi, R., et al. 2024, *Phys. Rev. D*, 110, 022001, doi: [10.1103/PhysRevD.110.022001](https://doi.org/10.1103/PhysRevD.110.022001)

Abbasi, R., et al. 2025, <https://arxiv.org/abs/2507.22233>

Abdollahi, S., Acero, F., Baldini, L., et al. 2022, *The Astrophysical Journal Supplement Series*, 260, 53, doi: [10.3847/1538-4365/ac6751](https://doi.org/10.3847/1538-4365/ac6751)

Adriani, O., et al. 2025a, *Phys. Rev. X*, 15, 031016, doi: [10.1103/yypk-zmb8](https://doi.org/10.1103/yypk-zmb8)

Adriani, O., et al. 2025b, <https://arxiv.org/abs/2511.13886>

Aguilar, J. A., et al. 2021, *JINST*, 16, P03025, doi: [10.1088/1748-0221/16/03/P03025](https://doi.org/10.1088/1748-0221/16/03/P03025)

Ai, S., & Gao, H. 2023, *Astrophys. J.*, 944, 115, doi: [10.3847/1538-4357/acb3bf](https://doi.org/10.3847/1538-4357/acb3bf)

Aiello, S., et al. 2025, *Nature*, 638, 376, doi: [10.1038/s41586-024-08543-1](https://doi.org/10.1038/s41586-024-08543-1)

Álvarez-Muñiz, J., et al. 2020, *Sci. China Phys. Mech. Astron.*, 63, 219501, doi: [10.1007/s11433-018-9385-7](https://doi.org/10.1007/s11433-018-9385-7)

Boncioli, D., Biehl, D., & Winter, W. 2019, *Astrophys. J.*, 872, 110, doi: [10.3847/1538-4357/aafda7](https://doi.org/10.3847/1538-4357/aafda7)

Campana, S., et al. 2006, *Nature*, 442, 1008, doi: [10.1038/nature04892](https://doi.org/10.1038/nature04892)

Chevalier, R. A., & Li, Z.-Y. 2000, *Astrophys. J.*, 536, 195, doi: [10.1086/308914](https://doi.org/10.1086/308914)

Duran, R. B., Nakar, E., Piran, T., & Sari, R. 2015, *Mon. Not. Roy. Astron. Soc.*, 448, 417, doi: [10.1093/mnras/stv011](https://doi.org/10.1093/mnras/stv011)

Evans, P. A., Beardmore, A. P., Page, K. L., et al. 2009, *Monthly Notices of the Royal Astronomical Society*, 397, 1177–1201, doi: [10.1111/j.1365-2966.2009.14913.x](https://doi.org/10.1111/j.1365-2966.2009.14913.x)

Fan, Y.-Z., Zhang, B.-B., Xu, D., Liang, E.-W., & Zhang, B. 2011, *Astrophys. J.*, 726, 32, doi: [10.1088/0004-637X/726/1/32](https://doi.org/10.1088/0004-637X/726/1/32)

Glaser, C., et al. 2020, *Eur. Phys. J. C*, 80, 77, doi: [10.1140/epjc/s10052-020-7612-8](https://doi.org/10.1140/epjc/s10052-020-7612-8)

Gupta, N., & Zhang, B. 2007, *Astropart. Phys.*, 27, 386, doi: [10.1016/j.astropartphys.2007.01.004](https://doi.org/10.1016/j.astropartphys.2007.01.004)

Hamidani, H., Sato, Y., Kashiyama, K., et al. 2025, arXiv e-prints, arXiv:2503.16243, doi: [10.48550/arXiv.2503.16243](https://doi.org/10.48550/arXiv.2503.16243)

Kotera, K., Mukhopadhyay, M., Alves Batista, R., et al. 2025, <https://arxiv.org/abs/2504.08973>

Kurashiki, N., Murase, K., & Santander, M. 2022, *Ann. Rev. Nucl. Part. Sci.*, 72, 365, doi: [10.1146/annurev-nucl-011122-061547](https://doi.org/10.1146/annurev-nucl-011122-061547)

Liang, E., Zhang, B., & Dai, Z. G. 2007, *Astrophys. J.*, 662, 1111, doi: [10.1086/517959](https://doi.org/10.1086/517959)

Liu, R.-Y., Wang, X.-Y., & Dai, Z.-G. 2011, *MNRAS*, 418, 1382, doi: [10.1111/j.1365-2966.2011.19590.x](https://doi.org/10.1111/j.1365-2966.2011.19590.x)

Liu, R.-Y., Zhang, H.-M., & Wang, X.-Y. 2023, *Astrophys. J. Lett.*, 943, L2, doi: [10.3847/2041-8213/acaf5e](https://doi.org/10.3847/2041-8213/acaf5e)

Margutti, R., Soderberg, A. M., Wieringa, M. H., et al. 2013, *The Astrophysical Journal*, 778, 18, doi: [10.1088/0004-637x/778/1/18](https://doi.org/10.1088/0004-637x/778/1/18)

Meszaros, P., & Rees, M. J. 1997, *Astrophys. J.*, 476, 232, doi: [10.1086/303625](https://doi.org/10.1086/303625)

Miceli, D., & Nava, L. 2022, *Galaxies*, 10, 66, doi: [10.3390/galaxies10030066](https://doi.org/10.3390/galaxies10030066)

Murase, K., Ioka, K., Nagataki, S., & Nakamura, T. 2006, *The Astrophysical Journal*, 651, L5–L8, doi: [10.1086/509323](https://doi.org/10.1086/509323)

Murase, K., Mukhopadhyay, M., Kheirandish, A., Kimura, S. S., & Fang, K. 2022, *Astrophys. J. Lett.*, 941, L10, doi: [10.3847/2041-8213/aca3ae](https://doi.org/10.3847/2041-8213/aca3ae)

Murase, K., Toma, K., Yamazaki, R., & Mészáros, P. 2011, *ApJ*, 732, 77, doi: [10.1088/0004-637X/732/2/77](https://doi.org/10.1088/0004-637X/732/2/77)

Naab, R., Ganster, E., & Zhang, Z. 2023, Measurement of the astrophysical diffuse neutrino flux in a combined fit of IceCube’s high energy neutrino data, <https://arxiv.org/abs/2308.00191>

Nava, L., Sironi, L., Ghisellini, G., Celotti, A., & Ghirlanda, G. 2013, *MNRAS*, 433, 2107, doi: [10.1093/mnras/stt872](https://doi.org/10.1093/mnras/stt872)

Navas, S., et al. 2024, *Phys. Rev. D*, 110, 030001, doi: [10.1103/PhysRevD.110.030001](https://doi.org/10.1103/PhysRevD.110.030001)

Sari, R., & Piran, T. 1995, *Astrophys. J. Lett.*, 455, L143, doi: [10.1086/309835](https://doi.org/10.1086/309835)

Sari, R., Piran, T., & Narayan, R. 1998, *Astrophys. J. Lett.*, 497, L17, doi: [10.1086/311269](https://doi.org/10.1086/311269)

Sawada, R., & Ashida, Y. 2025, *Astrophys. J.*, 982, 93, doi: [10.3847/1538-4357/adb721](https://doi.org/10.3847/1538-4357/adb721)

Senno, N., Murase, K., & Meszaros, P. 2016, *Phys. Rev. D*, 93, 083003, doi: [10.1103/PhysRevD.93.083003](https://doi.org/10.1103/PhysRevD.93.083003)

Sironi, L., Keshet, U., & Lemoine, M. 2015, *Space Sci. Rev.*, 191, 519, doi: [10.1007/s11214-015-0181-8](https://doi.org/10.1007/s11214-015-0181-8)

Soderberg, A. M., Kulkarni, S. R., Nakar, E., et al. 2006, *Nature*, 442, 1014–1017, doi: [10.1038/nature05087](https://doi.org/10.1038/nature05087)

Sun, H., Zhang, B., & Li, Z. 2015, *Astrophys. J.*, 812, 33, doi: [10.1088/0004-637X/812/1/33](https://doi.org/10.1088/0004-637X/812/1/33)

Sun, H., Liu, H.-Y., Pan, H.-W., et al. 2022, *Astrophys. J.*, 927, 224, doi: [10.3847/1538-4357/ac5328](https://doi.org/10.3847/1538-4357/ac5328)

Waxman, E., & Bahcall, J. 1997, *Phys. Rev. Lett.*, 78, 2292, doi: [10.1103/PhysRevLett.78.2292](https://doi.org/10.1103/PhysRevLett.78.2292)

Yoshida, S., & Murase, K. 2020, *Phys. Rev. D*, 102, 083023, doi: [10.1103/PhysRevD.102.083023](https://doi.org/10.1103/PhysRevD.102.083023)

Yoshida, S., & Murase, K. 2024, *Phys. Rev. D*, 110, 043045, doi: [10.1103/PhysRevD.110.043045](https://doi.org/10.1103/PhysRevD.110.043045)

Yuan, W., et al. 2025, *Sci. China Phys. Mech. Astron.*, 68, 239501, doi: [10.1007/s11433-024-2600-3](https://doi.org/10.1007/s11433-024-2600-3)

Zhang, B. 2018, *The Physics of Gamma-Ray Bursts* (Cambridge University Press)

Zhang, B. T., & Murase, K. 2023, *Mon. Not. Roy. Astron. Soc.*, 524, 76, doi: [10.1093/mnras/stad1829](https://doi.org/10.1093/mnras/stad1829)

Zhang, B. T., Murase, K., Ioka, K., & Zhang, B. 2025, *Journal of High Energy Astrophysics*, 45, 392–408, doi: [10.1016/j.jheap.2025.01.007](https://doi.org/10.1016/j.jheap.2025.01.007)

Zhang, B. T., Murase, K., Kimura, S. S., Horiuchi, S., & Mészáros, P. 2018, *Phys. Rev. D*, 97, 083010, doi: [10.1103/PhysRevD.97.083010](https://doi.org/10.1103/PhysRevD.97.083010)